Autophagy

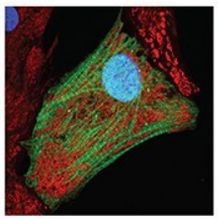

Autophagy

ISSN: (Print) (Online) Journal homepage: https://www.tandfonline.com/loi/kaup20

FNDC-1-mediated mitophagy and ATFS-1 coordinate to protect against hypoxia-reoxygenation

Yunki Lim, Brandon Berry, Stephanie Viteri, Matthew McCall, Eun Chan Park, Christopher Rongo, Paul S. Brookes & Keith Nehrke

To cite this article: Yunki Lim, Brandon Berry, Stephanie Viteri, Matthew McCall, Eun Chan Park, Christopher Rongo, Paul S. Brookes & Keith Nehrke (2021) FNDC-1-mediated mitophagy and ATFS-1 coordinate to protect against hypoxia-reoxygenation, Autophagy, 17:11, 3389-3401, DOI: 10.1080/15548627.2021.1872885

To link to this article: https://doi.org/10.1080/15548627.2021.1872885

AUTOPHAGY
2021, VOL. 17, NO. 11, 3389–3401
https://doi.org/10.1080/15548627.2021.1872885

Taylor & Francis
Taylor & Francis Group

RESEARCH PAPER

FNDC-1-mediated mitophagy and ATFS-1 coordinate to protect against hypoxia-reoxygenation

Yunki Lim[a], Brandon Berry[b], Stephanie Viteri[a], Matthew McCall[c], Eun Chan Park[d], Christopher Rongo[d], Paul S. Brookes[b,e], and Keith Nehrke[a,b]

[a]Medicine and Perioperative Medicine Departments, School of Medicine and Dentistry, University of Rochester Medical Center, Rochester, New York, USA; [b]Pharmacology and Physiology and Perioperative Medicine Departments, School of Medicine and Dentistry, University of Rochester Medical Center, Rochester, New York, USA;; [c]Biostatistics and Perioperative Medicine Departments, School of Medicine and Dentistry, University of Rochester Medical Center, Rochester, New York, USA;; [d]Department of Genetics , Waksman Institute/Rutgers University, Piscataway, New Jersey, USA; [e]Anesthesiology, and Perioperative Medicine Departments, School of Medicine and Dentistry, University of Rochester Medical Center, Rochester, New York, USA

ABSTRACT

Mitochondrial quality control (MQC) balances organelle adaptation and elimination, and mechanistic crosstalk between the underlying molecular processes affects subsequent stress outcomes. FUNDC1 (FUN14 domain containing 1) is a mammalian mitophagy receptor that responds to hypoxia-reoxygenation (HR) stress. Here, we provide evidence that FNDC-1 is the *C. elegans* ortholog of FUNDC1, and that its loss protects against injury in a worm model of HR. This protection depends upon ATFS-1, a transcription factor that is central to the mitochondrial unfolded protein response (UPRmt). Global mRNA and metabolite profiling suggest that *atfs-1*-dependent stress responses and metabolic remodeling occur in response to the loss of *fndc-1*. These data support a role for FNDC-1 in non-hypoxic MQC, and further suggest that these changes are prophylactic in relation to subsequent HR. Our results highlight functional coordination between mitochondrial adaptation and elimination that organizes stress responses and metabolic rewiring to protect against HR injury.

Abbreviations: AL: autolysosome; AP: autophagosome; FUNDC1: FUN14 domain containing 1; HR: hypoxia-reperfusion; IR: ischemia-reperfusion; lof: loss offunction; MQC: mitochondrial quality control; PCA: principle component analysis; PPP: pentonse phosphate pathway; proK (proteinase K);UPRmt: mitochondrial unfolded protein response; RNAi: RNA interference.

ARTICLE HISTORY
Received 12 August 2019
Revised 30 December 2020
Accepted 4 January 2021

KEYWORDS
C. elegans; hypoxia-reoxygenation (HR); metabolism; mitochondrial unfolded protein response (UPRmt); mitophagy

Introduction

Mitochondria are central to energy metabolism, calcium signaling, and intrinsic cell death [1], and the outcome of diseases from cancer to neurodegeneration is impacted by mitochondrial adaptation [2,3]. Conceptually, mitochondrial quality control (MQC) mechanisms act in concert to restore homeostasis or, when the damage becomes too severe, to recycle damaged organelles. In addition to their role in damage control, these mechanisms can alter susceptibility to ischemia-reperfusion (IR) injury [4,5].

The mitochondrial unfolded protein response (UPRmt) is an MQC mechanism that utilizes a mitochondrial-nuclear communication axis to combat protein aggregates in the mitochondrial matrix [6]. In *C. elegans*, this stress response is mediated primarily by the transcription factor ATFS-1 [7]. Regulated trafficking of ATFS-1 to the nucleus induces the expression of chaperones, detoxification enzymes, and alternative metabolic pathway components designed to alleviate the mitochondrial proteotoxic burden and reestablish organelle homeostasis [8]. Prior activation of the UPRmt protects against hypoxia-reoxygenation (HR) injury in the nematode *C. elegans*, consistent with the observation of protein aggregation induced by HR, while disruption of UPRmt signaling suppresses certain forms of preconditioning or "mitohormesis" that can occur in response to sublethal prophylactic stress [9,10].

When excess stress overwhelms compensatory responses, dysfunctional mitochondria need to be eliminated from the organelle pool [11]. This can be accomplished by mitophagy, which is a form of selective macroautophagy/autophagy (referred to as autophagy hereafter) that can occur through either ubiquitin- or receptor-mediated processes [6]. The segregation of damaged organelles by mitochondrial fission and subsequent inhibition of their fusion machinery influences their delivery to autophagosomes for recycling [12]. Although the UPRmt and mitophagy work together to combat stress [13], the precise mechanisms through which these different branches of MQC interact with each other is still unclear.

FUNDC (FUN14 domain containing 1) is a ubiquitin-independent hypoxic mitophagy receptor that interacts with a variety of proteins involved in coordinating mitochondrial fission and fusion to facilitate the delivery of defective

CONTACT Keith Nehrke keith_nehrke@urmc.rochester.edu Department of Medicine, University of Rochester Medical Center, Box 675, 601 Elmwood Avenue, Rochester, NY 14642, USA.
Supplemental data for this article can be accessed here.

mitochondria to autophagosomes [14,15]. Genetic ablation of *Fundc1* exacerbates cardiac IR injury in mice [16], and deficiency in another hypoxia-induced mitophagy receptor, BNIP3, has also been reported to increase hypoxia-induced cell death [17]. Hence, a consensus has emerged that the induction of mitophagy is beneficial by allowing organisms to avoid the detrimental consequences of IR.

Here, we employed *C. elegans* to begin interrogating the role of receptor-mediated mitophagy in moderating HR injury. We have identified *C. elegans* FNDC-1 as an ortholog of mammalian FUNDC1 and demonstrated that *fndc-1* loss of function (lof) reduces hypoxic mitophagy, albeit only at short (<8 h) incubation periods. However, contrary to our expectations based upon the mammalian phenotype, we found that *fndc-1* lof alleviates rather than exacerbates HR injury following longer (~20 h) incubation periods. Further dissection of the mechanisms underlying this protection unveiled an *atfs-1*-dependent compensation that acts prophylactically (before HR) to protect the animal from subsequent HR. RNAseq and LC-MS/MS were used to identify changes in the transcriptional and metabolic landscape that could contribute to HR protection. These results support a *fndc-1* lof baseline phenotype independent of hypoxic mitophagy that involves mitochondrial adaptation through ATFS-1. This model contributes to our understanding of how individual molecular mechanisms that support MQC functionally intersect to control stress response outcomes.

Results

FNDC-1 is located on the outer mitochondrial membrane

Mammals have two FUNDC (FUN14 domain containing) paralogs. FUNDC1 has been well-studied for its role as a hypoxic mitophagy receptor [18], whereas FUNDC2 is less well-studied [19]. The sole *C. elegans* FUNDC ortholog *fndc-1* regulates paternal mitochondria degradation [20], which is a type of ubiquitin-independent mitophagy that occurs immediately following fertilization [21]. However, it is yet unclear whether worm FNDC-1 also has a FUNDC1-like role in eliminating mitochondria that have been damaged by hypoxia [22]. In order to test this, we first examined FNDC-1 association with mitochondria in somatic tissues.

A single-copy FNDC-1 fusion reporter strain was created by inserting the coding sequence of the red fluorescent protein mRuby3 at the N-terminus of the endogenous *fndc-1* gene via CRISPR-Cas9 genome editing was expressed nearly ubiquitously, though at differing levels between tissues [20]. We confirmed that the red fluorescent signal reflects FNDC-1 expression and localization by demonstrating its reduction in most tissues following RNA interference (RNAi) targeting *fndc-1*, except for neurons, which are refractory to RNAi in worms (**Figure S1A**). The fusion strain had no overt phenotype (including an HR phenotype), suggesting that the protein is functional. The mRuby3::FNDC-1 chimeric protein co-localized with GFP-labeled mitochondria in body wall muscle, albeit incompletely (Figure 1A), and protein levels were broadly increased by non-lethal hypoxia (Figure 1B).

However, the relatively weak fluorescent signal from the single-copy *mRuby3::fndc-1* transgene motivated us to express FNDC-1 at much higher levels via a conventional extrachromosomal array. The *myo-3* promoter was used to restrict transgene expression to body wall muscle (**Figure S1B**). In this strain, the FNDC-1 signal was distinctly punctate but did not overlap with the labeled mitochondria – though it did appear to decorate the mitochondrial ends – and the mitochondria were themselves highly fragmented compared to wildtype controls (**Figure S1C**). This is consistent with the finding that overexpression of FUNDC1 causes mitochondrial fragmentation in mice [14]. While it is unlikely that the presumptive aggregates caused by overexpression of FNDC-1 reflect its normal intracellular distribution, the phenotypic similarity between overexpression in mammals and worms is consistent with conserved protein targeting, despite that lack of overt co-localization.

To more critically test the distribution of FNDC-1 expressed at physiological levels, whole cell lysates from the single-copy *mRuby3::fndc-1* strain were separated into cytosolic and mitochondria fractions – which may contain slight amounts of other membrane compartments. The mitochondrial fraction was then digested with proteinase K (proK). The samples were probed by immunoblot with antibodies to actin, mRuby3, or ATP5F1A/ATP5a (ATP-1 in *C. elegans*), a conserved subunit of complex V on the inner mitochondrial membrane. Exposed proteins on the outer mitochondrial membrane should be susceptible to digestion by proK, while proteins that are on the inner mitochondrial membrane or in the mitochondrial matrix should be resistant to digestion. FNDC-1 clearly co-purified with the mitochondrial fraction and was more susceptible to proK digestion than ATP-1 (Figure 1D). We have shown previously that with increased incubation time or detergent permeabilization, even ATP-1 is digested from intact mitochondria [23]. This is illustrated by the presence of an ATP-1 cleavage product with longer proK incubation (Figure 1D). However, the differential sensitivity to partial proK digestion, in combination with the previous results, is consistent with FNDC-1 outer mitochondrial membrane residence – akin to that of its mammalian counterpart.

FNDC-1 contributes to mitophagy in body wall muscle following short periods of HR

Mammalian FUNDC1 is activated under hypoxia by a series of signaling events that culminate in its receptor activity for mitophagy, the process of mitochondrial elimination through selective autophagy [16,24,25]. To assess the contribution of FNDC-1 to mitophagy in worms, a transgenic strain was created expressing mito-mKeima in the relatively alkaline mitochondrial matrix of body wall muscle, which simplifies imaging due to the physical structure of the tissue and is relevant to mammalian mitophagy [26]. Mito-mKeima is a protease-resistant, pH-sensitive fluorescent protein that has been used to monitor mitophagy through dual-excitation fluorescent imaging [27]. Following mitochondrial engulfment by autophagosomes (AP) and incorporation into autolysosomes (AL), acidic punctae form that are both

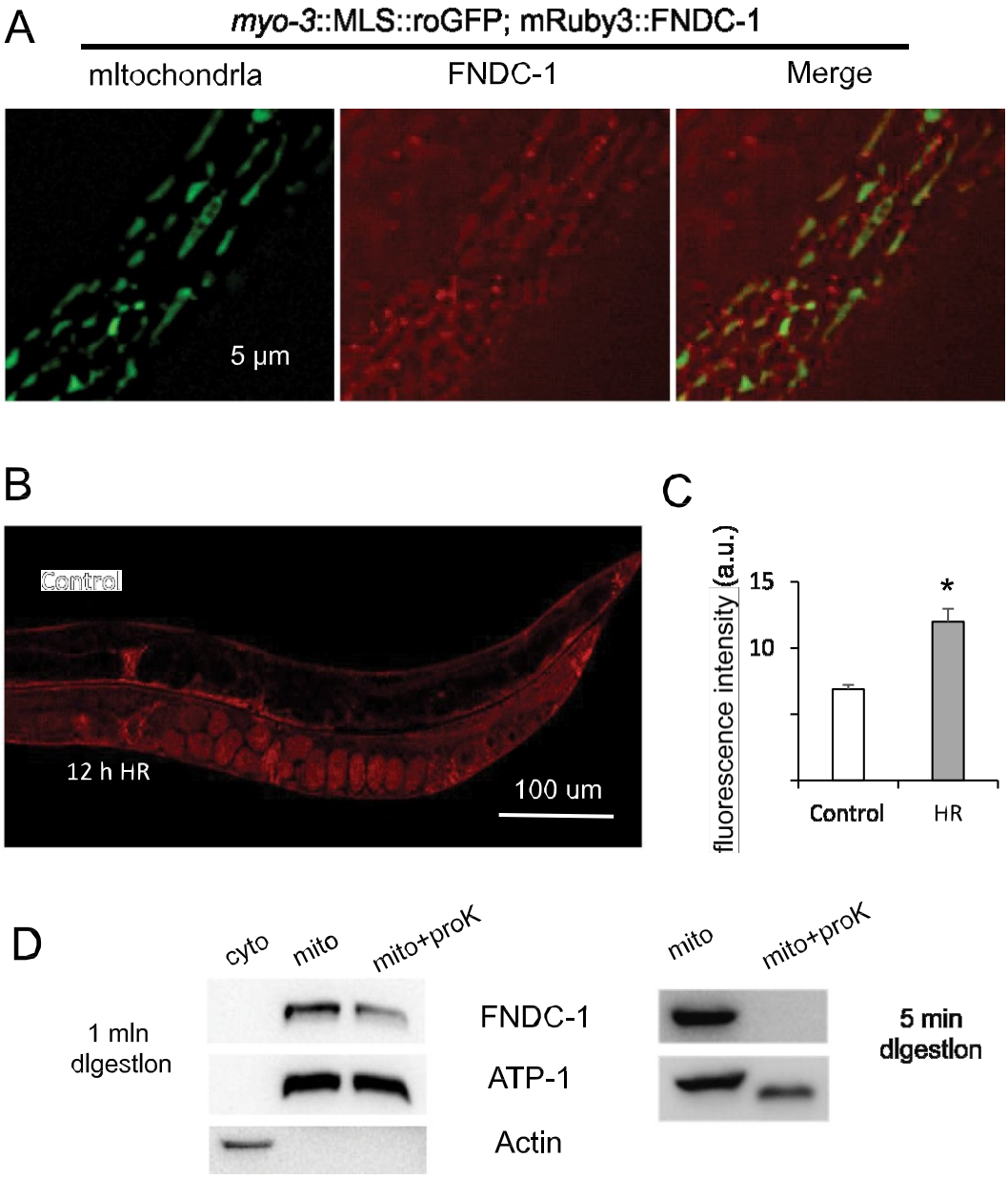

Figure 1. Transgenic FNDC-1 localization. (A) Fluorescent images of worms expressing mito-roGFP (green) and mRuby3::FNDC-1 (red), with an overlay of the two channels shown in Merge. Images are from a single confocal slice through body wall muscle. (B) Representative image of an animal expressing mRuby3::FNDC-1 under normoxic or HR conditions (0.1% > O_2, 12 h). (C) mRuby3 fluorescence intensity under normoxia or HR (n = 10; mean ± SEM; * $P < 0.05$, t-test). (D) Representative western blot analysis to assess protein targeting and susceptibility to protK digestion. A mitochondrial fraction from the mRuby3::FNDC-1 strain was subject to a proK protection assay and analyzed using an anti-mCherry antibody to detect the fusion protein. The matrix protein ATP-1 served as a control for mitochondrial outer membrane integrity, while the cytosolic protein Actin served to control for the purity of the mitochondrial fraction. Digestions were for 1 min or 5 min, as indicated. Three separate experimental replicates resulted in nearly identical results.

morphologically and spectrally distinct from mitochondria (Figure 2A). We refer to these acidified structures as mitolysosomes. Using these distinguishing features, mitophagy can be represented by either the volume ratio (pixel count) of mitolysosomes to mitochondria or by the number of mitolysosomes themselves (Materials and Methods). It is important to note that these metrics reflect a static distribution in the mitochondrial content of the cell rather than flux and do not provide mechanistic insight into the precise step in the mitophagy pathway that is impacted. Hence, apparent differences could reflect the rate of lysosomal degradation, declines in lysosomal pH, or even changes in mitochondrial membrane potential.

Starvation, HR, and aging have all been shown to influence autophagic flux in *C. elegans*, with strong induction observed in the intestine under HR [28,29]. Interestingly, all three conditions – including the well-established HR model that is functionally anoxic (O_2 < 0.1%) and slightly hyperthermic (26°C) – also influenced the distribution of muscle cell mito-mKeima in our transgenic strain (Figure 2 and Table S3). Baseline mitophagy was negligible in an N2 wild-type young adult background, but both the volume ratio and the number

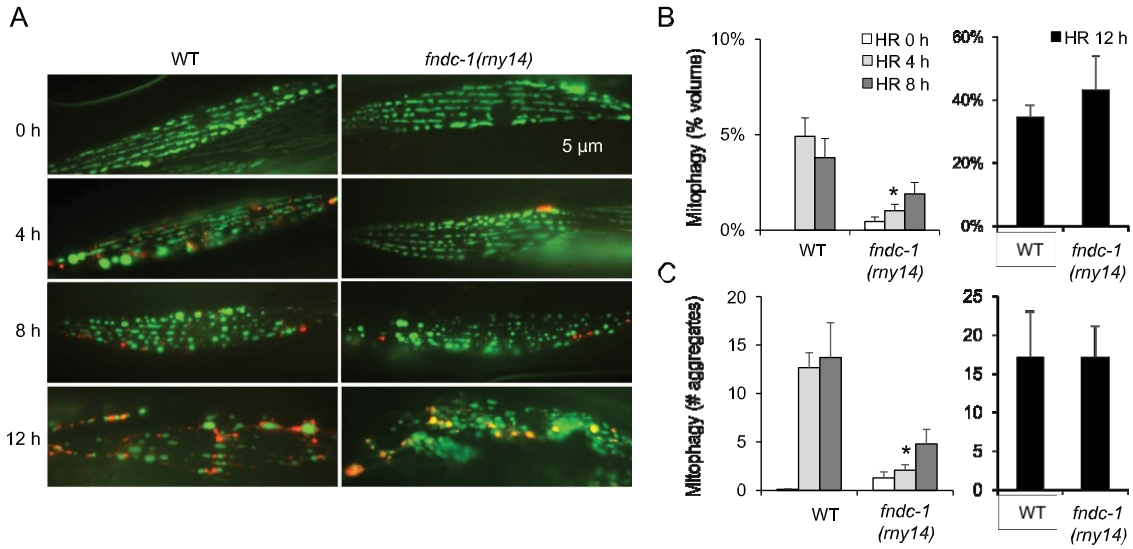

Figure 2. Delayed HR-induced mitophagy in the *fndc-1(rny14)* lof mutant. (A) N2 or *fndc-1(rny14)* mutant worms expressing mito-mKeima in body wall muscle cells were subject to HR for 0, 4, 8, or 12 h, and analyzed using fluorescence microscopy. Mitochondria are colored green, and mitochondria engulfed by lysosomes are colored red. Mitophagy was quantified with or without HR treatment as described. The measurements included: (B) the percentage of mitochondria that had undergone mitophagy based upon total fluorescent pixel count for each population and (C) the number of mitolysosomes > 10 pixels ($n \geq 10$ images per condition; mean ± SEM; * $P < 0.0002$, N2 vs. *fndc-1[rny14]*, Two-way ANOVA). The 12 h data is presented separately due to the magnitude of the volume response.

of mitolysosomes rose to easily measurable levels following either starvation, HR or aging (Figure 2 and Table S3). Moreover, these values increased dramatically in HR as the hypoxic period was extended from 4 to 12 h, though not in a linear fashion (Figure 2B,C). Periods beyond 12 h were not tested due to potential complications from lethality. Importantly, *atg-7*, which codes for the *C. elegans* ATG7 ortholog that is essential for autophagosome formation, was required for the formation of acidic mKeima-containing puncta (**Figure S3B and Table. S3**), confirming a higher level mechanistic conservation with autophagy. Together, these results suggest that mito-mKeima fluorescence is a useful surrogate for assessing changes in mitophagy in worms, as in mammals, albeit without the deeper insights of flux analysis and with the caveat that the regulation of mitophagy can be tissue-dependent.

We then interrogated conservation of function between mammalian FUNDC1 and worm FNDC-1 by examining hypoxic mitophagy in an *fndc-1* lof mutant strain [20]. The mutant was phenotypically normal under stereotypical laboratory conditions (**Figure S2A-C**), with a slight elevation in the ratio of mitochondrial to nuclear genomes (**Figure S2D**), and a normal mitochondrial redox status [30,31] (**Figure S2E**). Baseline body wall muscle mitophagy in the mutant was indistinguishable from the control strain (Figure 2 and Table S3). In contrast, *fndc-1* lof reduced HR-induced mitophagy following 4 h of hypoxia. However, this effect was restricted to short periods of hypoxia. By 8 h, the WT control and *fndc-1 (rny14)* mutant were statistically indistinguishable (Figure 2B, C), suggesting a delay in the process rather than its overt suppression, and by 12 h mitophagy had increased dramatically in both strains. Moreover, *fndc-1* lof also dramatically reduced body wall muscle mitophagy in aged worms but exacerbated starvation-induced mitophagy (**Table. S3**). While there was no significant difference in lifespan between control and the *fndc-1(rny14)* mutant (**Figure S2C**), these later data demonstrate that *fndc-1* affects MQC outside of its role in early HR responses, at least in body wall muscle.

Since mitophagy is a form of selective autophagy, additional experiments were conducted to assess bulk autophagy in the *fndc-1* lof strain. To accomplish this, we used a dual-fluorescent tandem tagged *mCherry::gfp::lgg-1* reporter where AP are visualized as puncta positive for both GFP and mCherry fluorescence, but AL emit only the mCherry signal due to quenching of GFP in the acidic environment [29]. While we noted a non-significant reduction in the number of AL compared to AP with increased hypoxia duration, at no time did the *fndc-1(rny14)* mutants differ significantly from the WT control (**Figure S3A**). These data suggest that the effect of *fndc-1* lof on hypoxic mitophagy is itself selective and does not extend more broadly to bulk autophagy – even though regulators of autophagy such as *atg-7* clearly impact mitochondrial clearance, and conditions that have been shown to stimulate autophagy also appear to stimulate mitophagy in body wall muscle.

ATFS-1 is central to HR protection in the fndc-1 *lof mutant*

HR in *C. elegans* (O_2 < 0.1%, 20 h at 26°C) has been used extensively to model IR injury, and in worms as in mammals, mitochondria are central arbiters of survival following IR, with MQC mechanisms contributing to cell fate [10,32–37]. Mice lacking *Fundc1* are relatively susceptible to IR injury [38], consistent with the idea that mitophagy is protective following IR. Hence, we were surprised to find that the *fndc-1* lof mutant was relatively resistant to HR, as well as oxidative and heat stress (**Figure S4**). We hypothesized that the *fndc-1* lof mutant might possess some form of adaptation.

We and others have shown that activation of the UPRmt protects worms against HR [9,10]. This protection can translate to other types of stress and even susceptibility to pathogen infection [39]. More recent work has extended this observation to mice by showing that activation of the UPRmt by doxycycline or oligomycin protects against cardiac IR [40]. The *C. elegans* gene *atfs-1* codes for a transcription factor that is central to the activation of the UPRmt [7]. *Atfs-1* lof prevents an adaptive response to stress that would otherwise protect against HR injury, while a gain-of-function allele (*et15*) elicits endogenous protection [9]. It is possible that mitochondria that would normally be targeted for degradation by FNDC-1 persist in the *fndc-1(rny14)* mutants, and that the persistent accumulation of damaged organelles could result in UPRmt activation and HR protection [41]. Data indicating that *fndc-1* contributes to aging-induced mitophagy support a role that is independent of hypoxia and provides a premise to test the hypothesis that *fndc-1* and *atfs-1* act together to suppress the detrimental effect of HR (**Table S3**).

Here, we employed epistasis between *fndc-1* and *atfs-1* to directly address this hypothesis. Epistasis is a genetic technique used to establish functional relationships between genes through their effect on a shared phenotype. We found that a loss-of-function *atfs-1(tm4525)* mutation suppressed the beneficial effect of *fndc-1(rny14)* on HR injury, while a gain-of-function *atfs-1(et15)* mutation phenocopied the effect, with no additional protection in response to *fndc-1(rny14)* (Figure 3A). Moreover, *atfs-1(tm4525)* also suppressed the reduction in hypoxic mitophagy exhibited in *fndc-1(rny14)* mutants (Figure 3B). Given that this reduction was only apparent at early incubation periods, its contribution to mortality following prolonged incubation is unclear. However, it is clear that

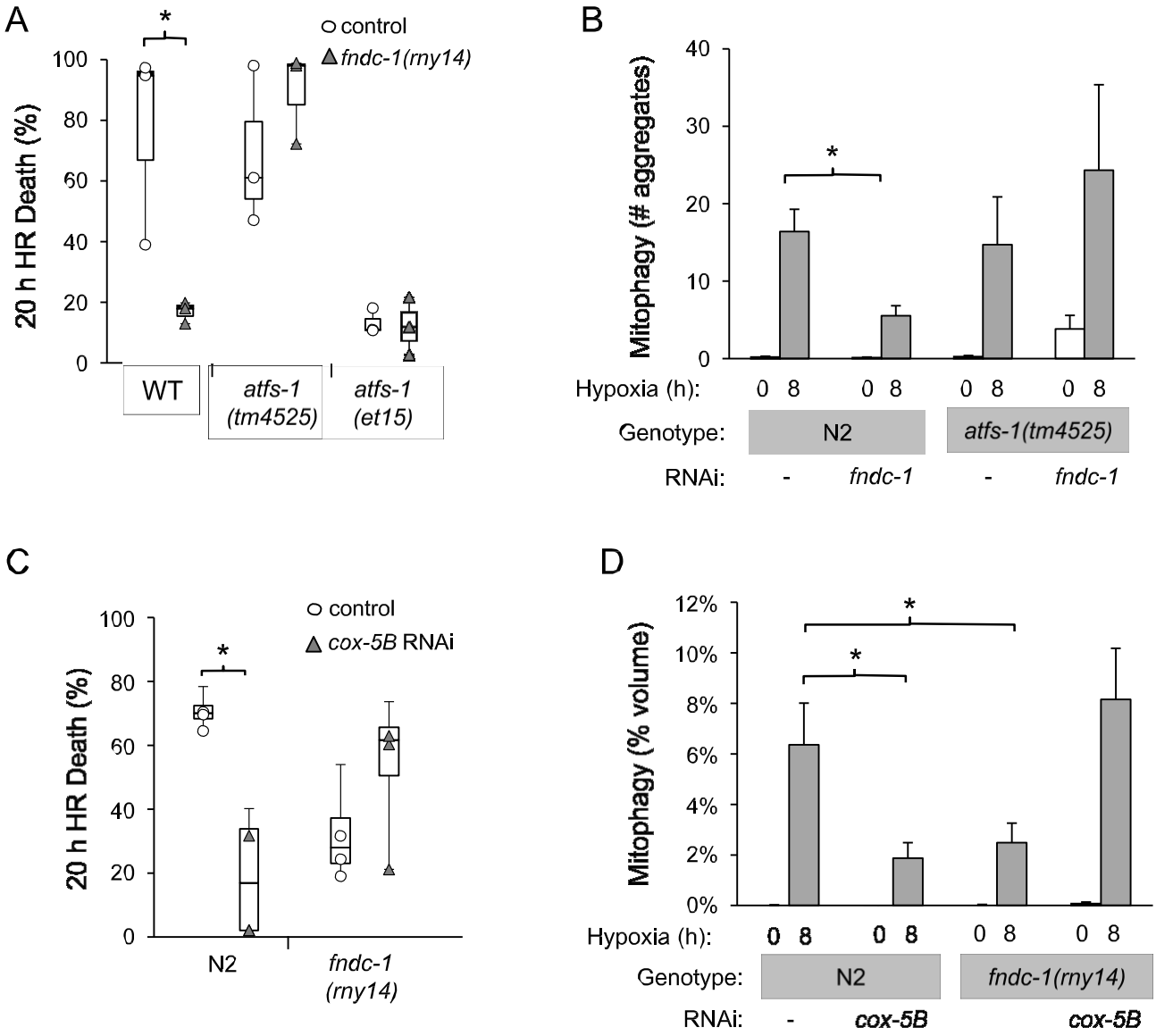

Figure 3. *Fndc-1* and *atfs-1* are epistatic for both HR-induced mitophagy and mortality. HR (< 0.1% oxygen and 26°C, with recovery at 20°C as indicated in the Methods) was for either (A, C) 20 h to measure mortality ($n \geq 50$ worms per replicate with each condition analyzed in parallel at the same time; mean ± SEM from three independent experiments performed on different days. * $P < 0.0063$, WT vs *fndc-1[rny14]*; Two-way ANOVA) or (B, D) 8 h to measure mitophagy ($n \geq 10$; mean ± SEM; * $P < 0.006$, Two-way ANOVA).

fndc-1 lof triggers protection through *atfs-1*-dependent mechanism(s).

The UPRmt shifts metabolism toward alternative energy sources and activates the expression of a variety of proteases, chaperones, autophagy factors, and detoxification enzymes in order to combat protein damage and reestablish proteostasis [3]. In *C. elegans*, several promoter GFP fusions have been used extensively to gauge activation of the UPRmt, with the most well-characterized being *hsp-6* (mitochondrial HSPA9/Hsp70) and *hsp-60* (HSPD1/Hsp60). Despite the requirement for *atfs-1* in HR protection following loss of *fndc-1*, neither of these reporters nor the endogenous *hsp-6* and *hsp-60* gene products were elevated in the *fndc-1(rny14)* mutant. (**Figure S5A and S5B**). Interestingly, positive control treatment with *cox-5B* RNAi to activate the UPRmt [9] induced expression of an *hsp-6*::GFP transgene in the *fndc-1* lof mutant at reduced levels compared to the wild-type background, and did not activate *hsp-60*::GFP expression at all (**Figure S5A**). Hence, the *fndc-1* lof mutant appears to be generally less responsive to mitochondrial stress.

In order to further interrogate the functional significance of this observation, we asked whether *cox-5B* RNAi treatment, which normally protects against subsequent mitochondrial stress, was effective in the *fndc-1(rny14)* strain, which is endogenously protected. Not only were the effects not additive, but *cox-5B* RNAi actually suppressed the effect of the *fndc-1* lof mutant as regards both HR injury and hypoxic mitophagy (Figure 3C,D). This result was somewhat counterintuitive, since it appeared that both the activation of the UPRmt (by *cox-5B* RNAi) and the inability to activate the UPRmt (in the *atfs-1* lof mutant) could suppress the *fndc-1* lof phenotypes. However, within this context, we note that compounding stressors can be maladaptive rather than beneficial. This caused us to wonder whether the loss of *fndc-1* compromises baseline, non-stress-induced mitophagy and imposes mild basal mitochondrial stress on the organism. If so, this could resolve the seemingly contradictory results, and might also underlie the reduced magnitude of the *cox-5B* RNAi-mediated response in the *fndc-1* lof mutant – indeed, UPRmt feedback mechanisms have been identified that dampen its subsequent responsiveness [39] to prevent chronic elevation.

Despite our inability to measure a change in mitophagy at baseline, there is some premise to support the idea that FNDC-1 contributes to ongoing MQC. Case in point, we observed a clear impairment in mitophagy in aged *fndc-1(rny14)* mutants, independent of hypoxia (**Table S3**). Based on these data, we hypothesized that mild stress resulting from *fndc-1(rny14)* might elicit non-canonical *atfs-1*-dependent pathways for adaptation, leading to an HR-protected phenotype.

Biochemical assays performed to decipher the physiologic nature of this response suggested that there was a slight decrease in protein carbonylation, a surrogate for oxidative stress, in *fndc-1* lof mutants, and no difference at all in either baseline or maximum oxygen consumption rates from any of the mutants, measured pre- or post-HR (**Figure S6**). Preliminary attempts to define relationships with other mitophagy regulators confirmed that regulators of mitochondrial morphologic dynamics were epistatic to *fndc-1*, but in general were mechanistically uninformative (**Figure S7 and Discussion**). Given these negative results, we were motivated to use more unbiased global screening approaches to identify potential mediators of the protected phenotype, including RNA sequencing and metabolomic profiling.

ATFS-1 contributes to changes to the transcriptional and metabolic landscape in a fndc-1 *lof mutant*

RNA-seq and ChIP-seq profiling has been used to identify stress response and metabolism genes regulated by the transcription factor ATFS-1 [8,42]. Since HR protection in the *fndc-1* lof mutant requires *atfs-1*, we profiled RNA expression using RNA-seq to identify putative targets that may contribute to the protected phenotype (Figure 4). To visualize the overall effect of experimental covariates and batch effects, we performed principal component analysis (PCA) and created a Venn diagram comparing differentially expressed genes (log2fold > 0.6; adjusted p-value ≤ 0.05) between genotypes (Figure 4A,B). PCA clearly indicated that the data was reproducible across biological and technical replicates, with *fndc-1 (rny14)* samples clustered separately from the N2 sample and *atfs-1(tm4525);fndc-1(rny14)* samples clustering much more closely to the N2 (Figure 4A). This is consistent with *atfs-1* being the principal arbiter of the *fndc-1* lof HR phenotype.

We found that the expression of 236 genes in the *fndc-1 (rny14)* mutant differed significantly from an N2 wildtype background (Figure 4B). Of these, 63 were also differentially expressed in the *fndc-1(rny14), atfs-1(tm4525)* double mutant compared to the *fndc-1* lof single mutant (Figure 4B). The overlap between data sets is expected to be enriched in genes that are regulated by ATFS-1 in response to *fndc-1* lof and to contribute to the *fndc-1* lof phenotype. The remaining genes would be predicted to be independently regulated by either *atfs-1* or *fndc-1*. *Fndc-1* dependent changes were analyzed individually using the DAVID online tool (http://david.abcc.ncifcrf.gov/home.jsp) [43,44], and the GO terms "innate immune response," "response to heat," and "lipid catabolic process" were highly enriched (Figure 4C). Interestingly, the UPRmt plays a profound role in innate immune responsiveness [45], and activation of the UPRmt can protect against pathogenic infection, heat stress, as well as HR [9,42,45].

Finally, we validated select RNA-seq results by assessing the transcriptional abundance of several genes from our data set that are associated with systemic stress responses and could reasonably be predicted to impact HR susceptibility. The small cysteine-rich peptide gene *sysm-1* (SYstemic Stress signaling Mediator) is regulated by the PMK-1/MAPK/p38 pathway and has been used to monitor innate immune responses using a fluorescent promoter fusion transgene [46]. As predicted from our analysis, *fndc-1* lof increased the expression of the *sysm-1* reporter even in a nonstressed environment (Figure 4D). Our RNA-seq analysis also suggested that *fndc-1* lof alters the expression of four *hsp-16* genes clustered on Chr V [47]. These genes code for small heat shock proteins in the alpha crystallin family that have been widely associated with stress as well as with defects in genes that detect and respond to stress in worms [48,49]. qRT-PCR confirmed that *hsp-16.1* and *hsp-16.48* expression were elevated in a *fndc-1* lof mutant background, and that this effect was suppressed by *atfs-1* lof (Figure 4E; please note that *hsp-*

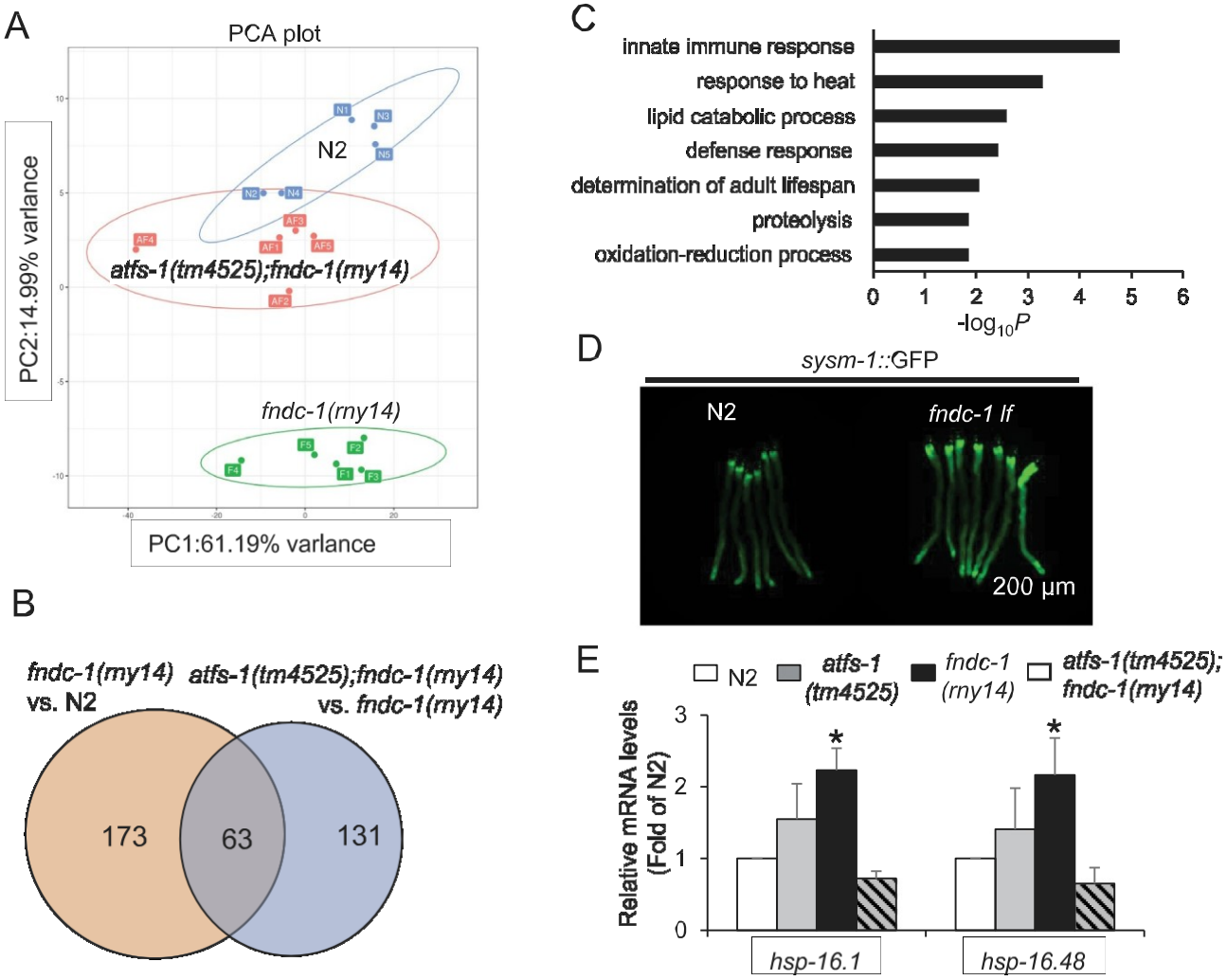

Figure 4. HR-independent transcriptional changes in the *fndc-1(rny14)* lof mutant. RNAseq was performed on five samples from each of three genotypes: N2, *fndc-1 (rny14)* lof, and *fndc-1(rny14), atfs-1(tm4525)* lof. (A) PCA was used to investigate replicate variability with three distinct clusters successfully identified. Each dot represents an individual sample and is colored according to genotype. (B) Venn diagram of the differentially expressed genes with an adjusted $P < 0.05$ from the *fndc-1(rny14)* versus N2 and the *atfs-1(tm4525);fndc-1(rny14)* versus *fndc-1(rny14)* analyses. (C) Gene ontology (GO) classification of the transcripts in the *fndc-1(rny14)* versus N2 differentially expressed genes in the Venn diagram. Bars indicate terms enriched for gene transcripts mapped to each GO category. All the statistically significant values of the terms were negative 10-base log-transformed. (D) Fluorescence images of the N2 and *fndc-1(rny14)* mutant animals containing the reporter *sysm-1*::GFP. (E) qRT-PCR analysis of normalized *hsp-16.1* and *hsp-16.48* relative expression levels as a function of genotype (n = 3; mean ± SEM; * $P < 0.05$, compared to the N2 control, One-way ANOVA).

16.49 and *hsp-16.11*, the other two genes in the cluster on Chr V, are duplications of *hsp-16.1* and *hsp-16.48*). As one might expect, *atfs-1* lof had little effect on its own. These data demonstrate that several genes whose expression has been linked to stress responses and damage mitigation are regulated by ATFS-1 in a *fndc-1* lof mutant. Although it is feasible that any one of these genes might individually modulate HR sensitivity, we feel it is more likely to be a combined repertoire of changes that lead to the protected phenotype.

Using a parallel approach, we next profiled the expression of over a hundred metabolites in methanol extracts from the mutant strains using LC-MS/MS. Figure 5A depicts a correlation heatmap and a hierarchical clustering of the top 25 metabolites that varied with genotype. As with the RNAseq analysis, the N2 and double mutant groups were more similar than the single *fndc-1(rny14)* mutant, suggesting an epistatic relationship between *fndc-1* and *atfs-1* in the context of the metabolome as well as the transcriptome.

One of the most intriguing hits was xanthine, a base generated from purine degradation to uric acid, which was significantly elevated in the *fndc-1* lof mutant. Xanthine has been shown to be a prosurvival metabolite for worms with mitochondrial dysfunction [50]. Taken together with metabolic pathway enrichment analysis (Figure 5B), there is reason to suspect that purine metabolism and the pentose phosphate pathway (PPP) may be affected by *fndc-1* lof, consistent with the involvement of these pathways in other models of mitochondrial metabolic rewiring [51,52].

Discussion

Mitochondrial degradation through various MQC mechan-

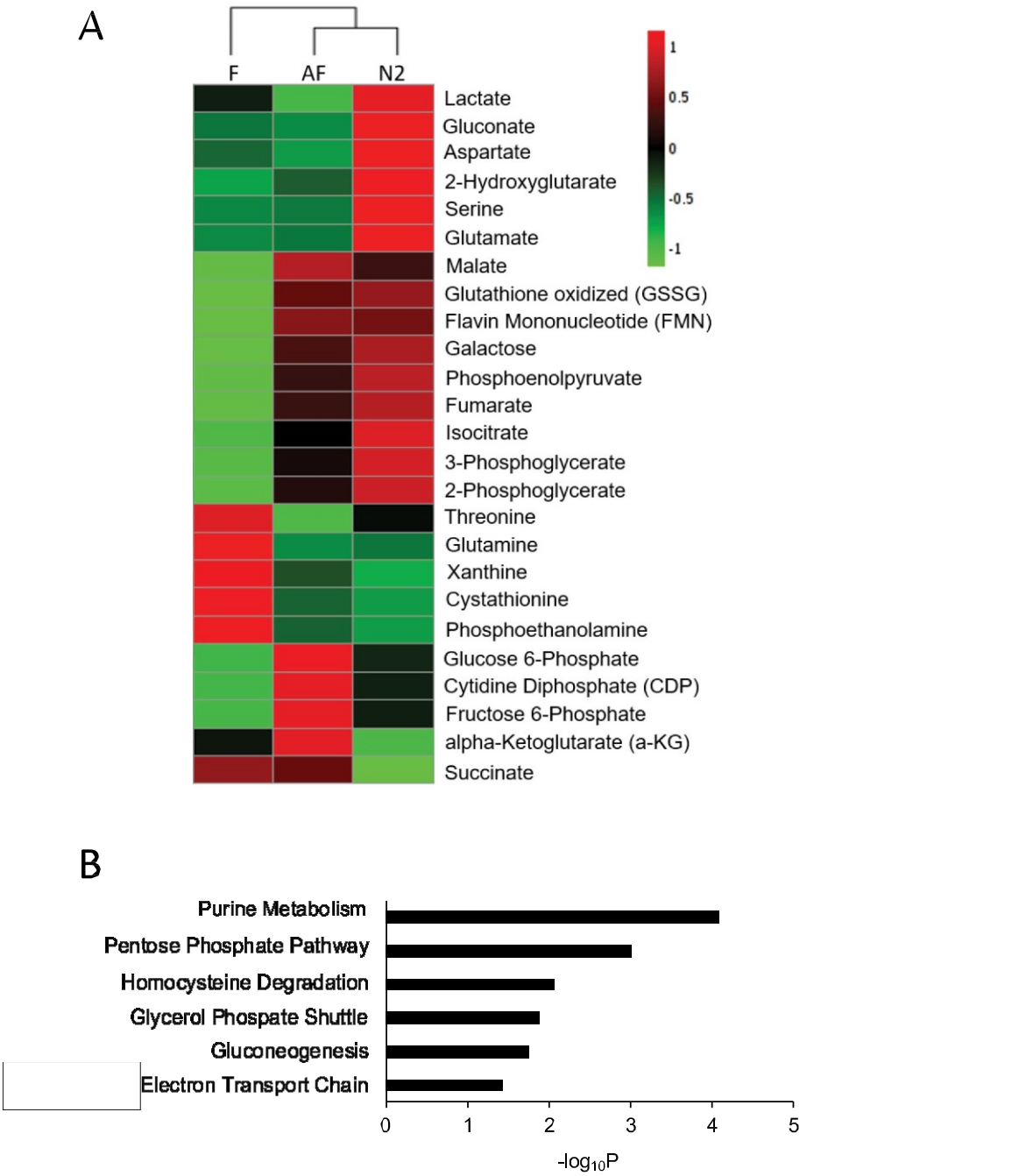

Figure 5. HR-independent metabolomic changes in the *fndc-1(rny14)* mutant. Metabolite profiling was performed on methanol extracts from N2, *fndc-1(rny14)* lof (F), and *atfs-1(tm4525), fndc-1(rny14)* lof (AF) mutant samples using LC-MS/MS. (A) Heat map (log2fold scale) showing a hierarchical clustering analysis of the top 25 metabolites that differ between genotypes (n = 4 samples per genotype). (B) Overrepresentation analysis of metabolite sets that are significantly different between N2 and *fndc-1(rny14)* worms.

organelle pool, to prevent damage from accumulating, and to maintain mitochondrial viability and function. The intersection between the UPRmt and mitophagy in regulating MQC has become increasingly appreciated as being relevant to health and disease [13]. The accepted view is that irreparable mitochondria are eliminated to prevent bad mitochondria from contaminating the organelle pool [41,53]. The fact that the *fndc-1(rny14)* phenotype described here is dependent in nearly all aspects on ATFS-1, the central transcription factor that regulates the UPRmt, suggests that an adaptive response is vital when elimination fails. Since mammalian FUNDC1 was originally annotated as a hypoxic mitophagy receptor, an important question is whether that response occurs before, during, or after HR.

Our results showing that activated stress responses and metabolic rewiring occur in the unstressed *fndc-1(rny14)* mutant (Figs. 4 and 5) suggest that FNDC-1 plays a role in baseline MQC in the absence of hypoxia, consistent with its stress-independent role during aging (**Table S3**). Whether these transcriptional and metabolic changes are independently protective or protective via their impact on HR-mediated

unlikely, given that mitophagy normalizes during HR by 12 h in the *fndc-1* lof mutant and several of the transcriptional and metabolic changes are predicted to contribute to protection on their own. Ultimately, while we can not deconvolve the impact of hypoxic mitophagy from the changes that precede hypoxia in terms of cause and effect, the most parsimonious explanation is that prophylaxis occurs prior to *de-facto* stress, as shown in the model in **Figure S8**.

However, there is almost certainly a requirement for some form of mitophagy in order to promote HR survival. Epistasis analysis to define genetic interactions between *fndc-1* and other mitophagy receptors, including the BNIP3 ortholog *dct-1*, and PINK1 and PRKN/parkin orthologs *pink-1* and *pdr-1* suggest that they are required, as least in part, for *fndc-1* lof-mediated HR protection (**Figure S7**). There is some precedence for functional compensation between receptors, as activation of BNIP3L/Nix is able to restore mitophagy in the absence of the PINK1-PRKN-mediated pathway [54]. Partial suppression of the *fndc-1* lof phenotype may suggest that these receptors are acting in concert, reflecting a broad need for some form of mitophagy following HR, as indicated in our model (**Figure S8**).

We also found that loss of the mitochondrial fusion protein MFN1/MFN2 ortholog FZO-1 blocks the beneficial effects of *fndc-1* RNAi and that loss of the fission-mediator DRP1 ortholog DRP-1 phenocopies *fndc-1* lof (**Figure S7A**). These data are consistent with the idea that mitochondrial dynamics and mitophagy can regulate each other to sustain mitochondrial network homeostasis. Further clarifying the precise regulatory mechanisms will likely take into account a link that has recently been established between defects in mitochondrial morphology and activation of the UPRmt [13].

The observation that the *fndc-1* lof mutant exhibits reduced sensitivity to UPRmt activation (**Figure S5**) is also consistent with our model. A feedback loop has been shown to be regulated by the transcription factor ZIP-3 that prevents sustained activation of the UPRmt [39]. We hypothesize that chronic low-level UPRmt induction in the *fndc-1* lof mutant could suppress subsequent responses to mitochondrial stress. This might also contribute to our observing a "non-canonical" profile of *atfs-1*-dependent targets that lack commonly used surrogates for UPRmt activation such as *hsp-6* and *hsp-60*.

We performed several screens to identify prospective constituents of this non-canonical response. Our data clearly demonstrate shifts in the metabolome and transcriptome when FNDC-1 is lost, and some of these changes can be predicted to alter hypoxic survival. For example, we noted increased expression of stress response genes, particularly those involved in innate immune and xenobiotic stress responses such as *sysm-1* and *hsp-16*. In addition, purine nucleotide metabolism and the PPP were among the top hits to emerge from our metabolomic screen.

There is a clear link between the PPP and hypoxia. This fundamental metabolic pathway plays a critical role in cellular redox homeostasis and metabolic reprogramming in cancer [55]. Similarly, xanthine – a purine base – has been shown to be a pro-survival metabolite in nematodes with mitochondrial dysfunction [50]. Xanthine accumulates in mitochondrial mutant worms when the insulin/insulin-like signaling pathway is inhibited, resulting in metabolic rewiring that compensates for mitochondrial dysfunction by saving ATP without restoring mitochondrial respiration [50].

In conclusion, our data support a model (**Figure S8**) describing functional coordination between mitophagy and MQC that impacts HR injury. The mechanism is likely to be the prophylactic remodeling of cell metabolism. Very recent work has shown that mammalian FUNDC1 interacts with HSPA8/HSC70 to promote cytosolic protein degradation and to stimulate AMP-activated protein kinase (AMPK) [56]. These data lend further weight to our conclusion that FNDC-1, which was originally annotated as a hypoxic mitophagy receptor, also functions to regulate basal mitochondrial metabolism. Future work should focus on defining precise details of that remodeling and how it integrates with signaling pathways that mediate cell survival.

Materials and methods

C. elegans strains and maintenance

Nematode strains (**Table S1**) were maintained at 20°C on *E. coli* OP50-seeded nematode growth media plates (3 g NaCl (Sigma Aldrich, S9888), 17 g agar (Thermo Fisher Scientific, DF0145), 2.5 g peptone (Sigma Aldrich, P6713), 1 ml cholesterol [5 mg ml-1 in 95% EtOH] (Sigma Aldrich, C3045), H_2O to 973 ml, autoclaved, and followed by the addition of sterile solutions: 1 ml 1 M $CaCl_2$ (Sigma Aldrich, C1016), 1 ml 1 M $MgSO_4$ (Sigma Aldrich, M7506), and 25 ml 1 M potassium phosphate [pH 6 by mixing mono (Sigma Aldrich, P0662) and di-basic (Sigma Aldrich, P8281) forms] according to standard protocols [57]. During revision of our manuscript, we found that a small deletion had occurred near the left arm of Chr X in the *fndc-1(rny14)* mutant strain, resulting in the loss of several exons in the transcript Y73B3A.4, which is a relatively unstudied gene that codes for a six-bladed beta-propeller, TolB-like protein. The mutation is not near a potential off-target crRNA binding site and may have arisen spontaneously, perhaps even during outcrossing (which was done 5x prior to our use of the *fndc-1* lof mutant). Nevertheless, we were able to generate independent strains that contained single mutations, and found that the HR phenotype cosegregated with *fndc-1* lof and not the Chr X mutation. For gene silencing, worms were fed HT115 bacteria (obtained from the *C. elegans* Genetic Center) transformed with control vector L4440 (courtesy of Dr. A. Fire, Stanford University) or vectors containing specific RNAi targets as described [58]. RNAi clones were from the Ahringer *C. elegans* RNAi feeding libraries and were induced and seeded onto nematode growth media plates containing 1 mM IPTG (Thermo Fisher Scientific, R0392).

Cloning

The *myo-3*::mito-mKeima vector pTFY7 was generated by using a PCR-amplified mito-mKeima CDS from pUC57-mito-mKeima vector (courtesy of Dr. C. Rongo, Rutgers

University) to replace an *Age*I-*Eco*RI fragment that codes for GFP in pKT104, which contains the *myo-3* promoter as a *Nhe*I-*Sac*II PCR fragment cloned into pFH6.II (courtesy of Dr. F. Hagen, University of Rochester). The *myo-3*::FUNDC-1::GFP vector pYI4 was generated by inserting a PCR-amplified *T06D8.7* genomic coding region into the *Acc65*I site of pKT104. To create transgenic strains, constructs were co-injected with the *pha-1*(+) rescue vector pC1 (courtesy of Dr. R. Schnabel, Technische Universität Braunschweig) into a *pha-1;him-5* mutant strain, and transformed worms were selected by survival at 20°C.

Q(RT)-PCR

qPCR was used to measure relative amounts of mitochondrial DNA and nuclear DNA as described [59], and qRT-PCR to quantify mRNA expression as follows: total RNA was extracted using the RNeasy kit (Qiagen, 74,134) and cDNA synthesized using the iScript cDNA synthesis kit (Bio-Rad, 1,708,890). qRT-PCR was performed using iTaq Universal SYBR® Green Supermix (Bio-Rad, 1,725,120) and CFX96 Touch Real-Time PCR Detection System (Bio-Rad Laboratories, Hercules, CA). Specific primers and targets are provided in **Table S2**. *hprt-1, y71g12b.10, fkh-10*, and *pmp-3* were used as normalization controls, and the ΔΔCt method was used to calculate gene expression levels.

Microscopy

In general, live specimens were mounted on 2% agar pads, paralyzed with 0.1% tetramisole in M9 buffer (3 g KH_2PO_4 (Sigma Aldrich, P0662), 6 g Na_2HPO_4 (Amresco, 348), 5 g NaCl (Sigma Aldrich, S9888), 1 ml 1 M $MgSO_4$ (Sigma Aldrich, M7506), H_2O to 1 liter), and imaged under coverslips. Most confocal images were acquired with a Nikon A1R HD confocal microscope (Nikon USA, Melville, NY) and NIS-Elements C software at the URMC Center for Advanced Light Microscopy and Nanoscopy. Confocal images of mRuby3::FNDC-1 were collected on a spinning disk confocal microscope system comprising a 100X Zeiss Plan-APOCHROMAT (1.4NA) oil lens (Carl Zeiss Microscopy, White Plains, NY), a CREST OPTICS X-Light^{TM} V2^{TP} Confocal Imager (Biovision Technologies, Exton, PA) illuminated by an 89NORTH LDI (89 North, Williston, VT), and a PRIME 95B sCMOS camera from Teledyne Photometrics (Tucson, AZ). Exposure times for mito-roGFP (Ex 470 nm/Em 525 nm) and mRuby3::FNDC-1 (Ex 555 nm/Em 640 nm) were 2 ms and 1000 ms, respectively. Images of nematodes expressing only mito-roGFP showed no bleedthrough of signal when collected with the same 555/640 settings. Epifluorescent microscopy was used for quantitative imaging of dual-excitation biosensors, including mito-mKeima and mito-roGFP1, as described previously [30]. Transgenic worms were imaged using a 40x oil objective on a rig consisting of a Nikon TE2000-U fluorescent microscope (Nikon USA, Melville, NY) connected to an LED light engine (Intelligent Imaging Innovations, Denver, CO) and an ORCA-Flash4.0 sCMOS Camera (Hamamatsu Photonics, Bridgewater, NJ), running SlideBook software (Intelligent Imaging Innovations, Denver, CO).

Mitochondrial fractionation and proK protection assay

Crude fractionation of *C. elegans* mitochondria was as described [60]. In brief, alkaline-bleach synchronized adult worms were harvested and washed 3x in ice-cold M9 buffer by centrifugation at 300 x g, 1 min. The washed worm pellets were resuspended in mitochondria isolation buffer (220 mM mannitol (Sigma Aldrich, M9847), 70 mM sucrose (Sigma Aldrich, S5016), 5 mM MOPS (Amresco, 0670), 2 mM EGTA (Sigma Aldrich, E3889), 0.4% BSA (Sigma Aldrich, A7030), pH 7.4) at 4°C. The worm cuticle was disrupted by grinding using an acid-washed mortar and pestle, followed by passage through a Dounce homogenizer. Debris was removed by low-speed centrifugation at 300 x g, 5 min. The resulting supernatant was then re-centrifuged at 7,000 x g, 10 min. The final supernatant was the cytosolic fraction, and the pellet was mitochondria. For submitochondrial localization studies, fractionated mitochondria were incubated in a buffer (20 mM HEPES (Sigma Aldrich, H3375), 1 mM EGTA (Sigma Aldrich, E3889), 10 mM PMSF (Sigma Aldrich, PMSF-RO), pH 7.2) with 2 uL of the 1:100 diluted proK (New England Biolabs, P8107S) for 5 min at room temperature.

Mitophagy and autophagy measurement

Mitochondrial monomeric Keima is a protease-resistant, pH-sensitive, dual-excitation fluorescent biosensor [27]. To measure mitophagy, transgenic worms expressing mito-mKeima in the body wall muscle were subject to HR in a 1-person gloveless anaerobic chamber (Coy Laboratory Products, Grass Lake, MI) for the period indicated in the figure legends, and allowed to recover overnight. Fluorescent emissions were collected through a 600-nm long-pass filter following sequential 440-nm and 550-nm excitation. At mitochondrial matrix pH, the 440-nm excitation signal predominates, whereas inside acidified AL, the 550-nm signal should predominate. However, a slight spectral overlap and pH-independent photoconversion were noted following prolonged illumination at 440-nm. To circumvent this issue, our analysis considered only pixels that fell into the top two-thirds of the intensity histogram for each channel and at the same time fell into the bottom third for the remaining channel. This threshold method prevented pixels with intermediate ratios, which could arise from spectral overlap or photoconversion, from contributing to the analysis. Once pixels that met our criteria were identified, a further threshold of 10 pixels minimum size was applied. From these final selections, "volume" (pixel number) and "count" (number of objects that meet the threshold standards) were determined from a single body wall muscle cell. Image analysis of mitophagy was performed blindly. Autophagy was quantified using *sqIs11[lgg-1p::mCherry::GFP::lgg-1 + rol-6]* following the previously described [29]. GFP- and mCherry-positive puncta were counted in the whole body using a Nikon A1R HD confocal microscope rig as described above in one 0.6 mm optical section.

thought to contribute to a bulk renewal of the

Survival assay

For heat stress, young adult hermaphrodites were incubated at 37°C for 2 h, and survival was measured following overnight recovery at 20°C. For oxidative stress, worms were incubated for 6 h at 20°C in M9 buffer containing *tert*-butyl hydroperoxide (Sigma Aldrich, 416,665)at a final concentration of 7 mM. For HR, worms were incubated in a 1-person gloveless anaerobic chamber (Coy Laboratory Products, Grass Lake, MI) with O_2 < 0.1% for 20 h (OP50) or 22 h (HT115) at 26°C and reoxygenated for 24 h at 20°C as previously described [9]. Each experimental replicate contained at least 50 adults, matched to controls that were run simultaneously. Hence, each graph of HR survival represents the average of multiple replicates where the experimental variables (e.g., genotype, RNAi) were always run in parallel.

Western blotting

For lysates, synchronized young adult worms were harvested by washing with ice-cold M9 buffer and centrifuged at 1,000 x g. The pellet was sonicated in lysis buffer (20 mM Tris-HCl (Sigma Aldrich, T5941), 100 mM NaCl (Sigma Aldrich, S9888), 1 mM EDTA (Sigma Aldrich, E9884), 1 mM DTT (Sigma Aldrich, D0632), 10% glycerol (J.T. Baker, 2136), 0.1% SDS (Sigma Aldrich, L3771), HALT™ protease inhibitor cocktail (Thermo Fisher Scientific, 78,430), pH 7.6). The worm lysates were combined with 5x SDS-PAGE sample buffer and heated for 10 min at 95°C. Proteins from the worm lysates were resolved on 10% SDS-PAGE, transferred to PVDF membrane (Bio-Rad, 1,620,177) and incubated with the primary antibody against anti-ATP5F1A/ATP5A (Abcam, ab14748), anti-mCherry (Thermo Fisher Scientific, PA5-34,974), anti-ACTB (Abcam, ab8226) and appropriate HRP-conjugated secondary antibodies (Cell Signaling Technology, 7076 and Jackson ImmunoResearch, 11–035-144).

Whole organism oxygen consumption

Oxygen consumption was measured using a Clark-type oxygen electrode (S1 electrode disc, DW2/2 electrode chamber and Oxy-Lab control unit, Hansatech Instruments, Norfolk UK). Synchronized 1-day adult animals were collected in M9 buffer, washed, and pelleted by centrifugation as described above. Animals were added to the electrode chamber in rapidly stirring 0.5 mL of M9 buffer and the oxygen consumption rate was measured. FCCP (Enzo Life Sciences, 370–86-5) was added to a final concentration of 160 µM to induce maximal respiration, and sodium azide (Sigma Aldrich, 71,289) was added to a final concentration of 40 mM to inhibit mitochondrial respiration. Each rate of oxygen consumption (basal, maximal, and inhibited) was measured for 6 minutes or until stable. Animals were then collected for protein quantification by the Folin-phenol method.

Oxyblot

Alkaline-bleach synchronized adult worms were harvested and washed 3x in ice-cold M9 buffer by centrifugation at 300 x g, 1 min. Protein carbonylation was assessed using an OxyBlot™ Protein Oxidation Detection Kit (Sigma-Aldrich, S7150). Proteins are the main target of ROS, and oxidized proteins introduce carbonyl groups at site-specific residues. The carbonyl groups are derivatized to 2,4-dinitrophenylhydrazone (DNP-hydrazone) by reaction with 2,4-dinitrophenylhydrazine (DNPH), which can be detected by western blotting with a DNP-specific antibody according to the manufacturer's protocol. The worm lysate (10 µg) was resolved on 10% gel SDS-PAGE, transferred to PVDF, and immunoblotted using primary antibodies against DNP or GAPDH (loading control; Cell Signaling Technology, 97,166).

RNA-seq

Samples were collected for five independent biological replicates obtained for each condition. Total RNA from synchronized young adult worms was extracted using TRIzol (Invitrogen, 15,596,018). The total RNA concentration was determined with a Nanodrop 1000 spectrophotometer (Thermo Fisher Scientific, Walthom, MA) and RNA quality assessed with an Agilent Bioanalyzer (Agilent, Santa Clara, CA). The TruSeq Stranded mRNA Sample Preparation Kit (Illumina, RS-122-2101) was used for next-generation sequencing library construction per manufacturer's protocols. Single end reads of 50 nt were generated for each sample using Illumina's HiSeq2500v4 platform (Illumina, San Diego, CA). Raw reads generated from Illumina HiSeq2500 sequencing were de-multiplexed using bcl2fastq version 1.8.4. DESeq2-1.16.1 within R-3.4.1 was used to perform data normalization and differential expression analysis with an adjusted p-value threshold of 0.05 on each set of raw expression measures [61]. The "lfcShrink" method was applied, which moderates log2 fold-changes for lowly expressed genes. The PCA was analyzed using pcaExplorer (https://github.com/federicomarini/pcaExplorer) with the DESeq2 normalized data and results [62]. Raw and processed data were submitted to GEO (accession GSE158628).

Metabolite analysis by LC-MS/MS

Age synchronized day 1 adult worm samples were harvested into tubes filled with glass beads and 80% methanol. The samples were bead-beaten at maximum speed for 30 s, followed by centrifugation at 300 x g for 4 min at 4°C, evaporated under N_2, and resuspended in 100 µL of 50% methanol. LC-MS/MS analysis was as previously described [63]. Metabolites were resolved by HPLC on a Prominence 20 system (Shimadzu USA, Colombia, MD), with a 150 × 2 mm Synergi Polar-RP column (Phenomenex, Torrance, CA) at 20°C. Metabolites were identified by single reaction monitoring on a triple-quadrupole Quantum TSQ mass spectrometer (Thermo Fisher Scientific, Walthom, MA). Data were analyzed using a publicly available MzRock machine learning tool kit (http://code.google.com/p/mzrock/). Selected metabolites were also analyzed using XCalibur Qual Browser (Thermo Fisher Scientific, Walthom, MA). The concentration of the protein extract was measured by BCA protein analysis (Thermo Fisher Scientific, 23,227) for normalization.

Metabolomics data analysis was performed using the MetaboAnalyst 2.0 [64].

Statistical analyses

Statistical significance was calculated with Prism 8 (GraphPad Software, San Diego, CA) or Excel (Microsoft, Redmond, WA). Data were analyzed using *t*-test, one-way ANOVA with Tukey test, two-way ANOVA with Holm-Sidak method for multiple comparisons, or log-rank test as indicated in the figure legends.

Acknowledgments

Several strains were obtained from the *Caenorhabditis Genetic Center*. Technical assistance was provided by Teresa Sherman and Sarah Fisher. This work was supported by USPHS grants R01HL127891 (KN, PSB); R01NS092558 (BB); R01GM101972 and R21NS102780 (EP, CR); R01HL071158 (PSB), NSF IOS1753742 (KN) and a Predoctoral Fellowship from the American Heart Association 18PRE33990054 (BB).

Disclosure statement

All authors declare no conflict of interest.

Funding

This work was supported by the National Institutes of Health [R01HL127891, R01NS092558, R01GM101972, R01HL071158 and R21NS102780], the National Science Foundation [IOS1753742], and a Predoctoral Fellowship from the American Heart Association [18PRE33990054].

ORCID

Brandon Berry http://orcid.org/0000-0002-2206-7615
Eun Chan Park http://orcid.org/0000-0002-6147-4088
Christopher Rongo http://orcid.org/0000-0002-1361-5288
Keith Nehrke http://orcid.org/0000-0001-9697-726X

References

[1] Vakifahmetoglu-Norberg H, Ouchida AT, Norberg E. The role of mitochondria in metabolism and cell death. Biochem Biophys Res Commun. 2017;482:426–431.
[2] Ploumi C, Daskalaki I, Tavernarakis N. Mitochondrial biogenesis and clearance: a balancing act. Febs J. 2017;284:183–195.
[3] Qureshi MA, Haynes CM, Pellegrino MW. The mitochondrial unfolded protein response: signaling from the powerhouse. J Biol Chem. 2017;292:13500–13506.
[4] Tahrir FG, Langford D, Amini S, et al. Mitochondrial quality control in cardiac cells: mechanisms and role in cardiac cell injury and disease. J Cell Physiol. 2019;234:8122–8133.
[5] Zhang J, Nadtochiy SM, Urciuoli WR, et al. The cardioprotective compound cloxyquin uncouples mitochondria and induces autophagy. Am J Physiol - Hear Circ Physiol. 2016;310:H29–H38.
[6] Pickles S, Vigié P, Youle RJ. Mitophagy and quality control mechanisms in mitochondrial maintenance. Curr Biol. 2018;28:R142–R143.
[7] Nargund AM, Pellegrino MW, Fiorese CJ, et al. Mitochondrial import efficiency of ATFS-1 regulates mitochondrial UPR activation. Science. 2012;337:587–590.
[8] Nargund AM, Fiorese CJ, Pellegrino MW, et al. Mitochondrial and nuclear accumulation of the transcription factor ATFS-1 promotes OXPHOS recovery during the UPRmt. Mol Cell. 2015;58:123–133.
[9] Peña S, Sherman T, Brookes PS, et al. The mitochondrial unfolded protein response protects against anoxia in *Caenorhabditis elegans*. PLoS One. 2016;11:1–16.
[10] Kaufman DM, Michael C, Kaufman DM, et al. Mitochondrial proteostatic collapse leads to hypoxic injury report mitochondrial proteostatic collapse leads to hypoxic injury. *Curr Biol*; 25:2171–2176.
[11] Runkel ED, Baumeister R, Schulze E. Mitochondrial stress: balancing friend and foe. Exp Gerontol. 2014;56C:194–201.
[12] Yoo S-M, Jung Y-K, Molecular A. Approach to mitophagy and mitochondrial dynamics. Mol Cells. 2018;41:18–26.
[13] Haeussler S, Köhler F, Witting M; Haeussler S, Köhler F, Witting M, et al. Autophagy compensates for defects in mitochondrial dynamics. PLoS Genet. 2020;16:e1008638.
[14] Wu S, Lu Q, Wang Q, et al. Binding of FUN14 domain containing 1 with inositol 1,4,5-trisphosphate receptor in mitochondria-associated endoplasmic reticulum membranes maintains mitochondrial dynamics and function in hearts in vivo. Circulation. 2017;136:2248–2266.
[15] Wu W, Lin C, Wu K, et al. FUNDC1 regulates mitochondrial dynamics at the ER-mitochondrial contact site under hypoxic conditions. Embo J. 2016;35:1368–1384.
[16] Zhou H, Zhu P, Wang J, et al. Pathogenesis of cardiac ischemia reperfusion injury is associated with CK2α-disturbed mitochondrial homeostasis via suppression of FUNDC1-related mitophagy. Cell Death Differ. 2018;25:1080–1093.
[17] Tracy K, Dibling BC, Spike BT, et al. BNIP3 is an RB/E2F target gene required for hypoxia-induced autophagy. Mol Cell Biol. 2007;27(17):6229–6242.
[18] Liu L, Feng D, Chen G, et al. Mitochondrial outer-membrane protein FUNDC1 mediates hypoxia-induced mitophagy in mammalian cells. Nat Cell Biol. 2012;14:177–185.
[19] Ma Q, Zhu C, Zhang W, et al. Mitochondrial PIP3-binding protein FUNDC2 supports platelet survival via AKT signaling pathway. Cell Death Differ. 2019;26:321–331.
[20] Lim Y, Rubio-Peña K, Sobraske PJ, et al. *Fndc-1* contributes to paternal mitochondria elimination in *C. elegans*. Dev Biol. 2019;454:15–20.
[21] Molina P, Lim Y, Boyd L. Ubiquitination is required for the initial removal of paternal organelles in *C.elegans*. Dev Biol. 2019;453:168–179.
[22] Kuang Y, Ma K, Zhou C, et al. Structural basis for the phosphorylation of FUNDC1 LIR as a molecular switch of mitophagy. Autophagy. 2016;12:2363–2373.
[23] Trewin AJ, Bahr LL, Almast A, et al. Mitochondrial reactive oxygen species generated at the complex-ii matrix or intermembrane space microdomain have distinct effects on redox signaling and stress sensitivity in *Caenorhabditis elegans*. Antioxid Redox Signal. 2019;31:594–607.
[24] Chen Z, Liu L, Cheng Q, et al. Mitochondrial E3 ligase MARCH5 regulates FUNDC1 to fine-tune hypoxic mitophagy. EMBO Rep. 2017;18:495–509.
[25] Wu H, Xue D, Chen G, et al. The BCL2L1 and PGAM5 axis defines hypoxia-induced receptor-mediated mitophagy. Autophagy. 2014;10:1712–1725.
[26] Vainshtein A, Desjardins EM, Armani A, et al. PGC-1α modulates denervation-induced mitophagy in skeletal muscle. Skelet Muscle. 2015;5:9.
[27] Katayama H, Kogure T, Mizushima N, et al. A sensitive and quantitative technique for detecting autophagic events based on lysosomal delivery. Chem Biol. 2011;18:1042–1052.
[28] Chapin HC, Okada M, Merz AJ, et al. Tissue-specific autophagy responses to aging and stress in *C. elegans*. Aging (Albany NY). 2015;7:419–434.
[29] Chang JT, Kumsta C, Hellman AB, et al. Spatiotemporal regulation of autophagy during *Caenorhabditis elegans* aging. Elife. 2017;6:1–23.

[30] Johnson D, Nehrke K. Mitochondrial fragmentation leads to intracellular acidification in *Caenorhabditis elegans* and mammalian cells. Mol Biol Cell. 2010;21:2191–2201.
[31] Hanson GT, Aggeler R, Oglesbee D, et al. Investigating mitochondrial redox potential with redox-sensitive green fluorescent protein indicators. J Biol Chem. 2004;279:13044–13053.
[32] Scott BA; Scott B a, Avidan MS, Crowder CM. Regulation of hypoxic death in. Regulation of hypoxic death in *C. elegans* by the Insulin/IGF receptor homolog DAF-2. Science. 2002;296:2388–2391.
[33] Zuckerman B, Abergel Z, Zelmanovich V, et al. Free radical biology and medicine characterization of gene expression associated with the adaptation of the nematode *C. elegans* to hypoxia and reoxygenation stress reveals an unexpected function of the neuroglobin GLB-5 in innate immunity. Free Radic Biol Med. 2017;108:858–873.
[34] Vozdek R, Long Y, Ma DK. The receptor tyrosine kinase HIR-1 coordinates HIF-independent responses to hypoxia and extracellular matrix injury. Sci Signal. 2018;11:eaat0138.
[35] Wojtovich AP, Sherman TA, Nadtochiy SM, et al. SLO-2 Is Cytoprotective and Contributes to Mitochondrial Potassium Transport. PLoS One. 2011;6:e28287.
[36] Wojtovich AP, Smith CO, Urciuoli WR, et al. Cardiac Slo2.1 is required for volatile anesthetic stimulation of k+ transport and anesthetic preconditioning. Anesthesiology. 2016;124:1065–1076.
[37] Anzell AR, Maizy R, Przyklenk K, et al. Mitochondrial quality control and disease: insights into ischemia-reperfusion injury. Mol Neurobiol. 2018;55:2547–2564.
[38] Zhang W, Ren H, Xu C, et al. Hypoxic mitophagy regulates mitochondrial quality and platelet activation and determines severity of I/R heart injury. Elife. 2016;5:71–86.
[39] Deng P, Naresh NU, Du Y, et al. Mitochondrial UPR repression during *Pseudomonas aeruginosa* infection requires the bZIP protein ZIP-3. Proc Natl Acad Sci U S A. 2019;116:6146–6151.
[40] Wang YT, Lim Y, McCall MN, et al. Cardioprotection by the mitochondrial unfolded protein response (UPR ^{mt}) requires ATF5. Am J Physiol Circ Physiol. 2019(ajpheart.00244.2019). DOI:10.1152/ajpheart.00244.2019
[41] Schulz AM, Haynes CM. UPRmt-mediated cytoprotection and organismal aging. Biochim Biophys Acta - Bioenergy. 2015;1847:1448–1456.
[42] Wu Z, Senchuk MM, Dues DJ, et al. Mitochondrial unfolded protein response transcription factor ATFS-1 promotes longevity in a long-lived mitochondrial mutant through activation of stress response pathways. BMC Biol. 2018;16:147.
[43] Huang DW, Sherman BT, Lempicki RA. Bioinformatics enrichment tools: paths toward the comprehensive functional analysis of large gene lists. Nucleic Acids Res. 2009;37:1–13.
[44] Huang DW, Sherman BT, Lempicki RA. Systematic and integrative analysis of large gene lists using DAVID bioinformatics resources. Nat Protoc. 2009;4:44–57.
[45] Pellegrino MW, Nargund AM, Kirienko NV, et al. Mitochondrial UPR-regulated innate immunity provides resistance to pathogen infection. Nature. 2014;516:414–417.
[46] Youngman MJ, Rogers ZN, Kim DHA. Decline in p38 MAPK signaling underlies immunosenescence in *Caenorhabditis elegans*. PLoS Genet. 2011;7:e1002082.
[47] Candido EP, Jones D, Dixon DK, et al. Structure, organization, and expression of the 16-kDa heat shock gene family of *Caenorhabditis elegans*. Genome. 1989;31:690–697.
[48] Matilainen O, Sleiman MSB, Quiros PM, et al. The chromatin remodeling factor ISW-1 integrates organismal responses against nuclear and mitochondrial stress. Nat Commun. 2017;8. Epub ahead of print. DOI:10.1038/s41467-017-01903-8
[49] Johnson JR, Rajamanoharan D, McCue H, et al. Small heat shock proteins are novel common determinants of alcohol and nicotine sensitivity in *Caenorhabditis elegans*. Genetics. 2016;202:1013–1027.
[50] Gioran A, Piazzesi A, Bertan F, et al. Multi-omics identify xanthine as a pro-survival metabolite for nematodes with mitochondrial dysfunction. Embo J. 2019;38:e99558.
[51] Cannino G, Ciscato F, Masgras I, et al. Metabolic plasticity of tumor cell mitochondria. Front Oncol. 2018;8. Epub ahead of print. DOI:10.3389/fonc.2018.00333
[52] Podrini C, Cassina L, Boletta A. Metabolic reprogramming and the role of mitochondria in polycystic kidney disease. Cell Signal. 2020;67:109495.
[53] Lin YF, Haynes CM. Metabolism and the UPRmt. Mol Cell. 2016;61:677–682.
[54] Koentjoro B, Park J-S, Sue CM. Nix restores mitophagy and mitochondrial function to protect against PINK1/Parkin-related Parkinson's disease. Sci Rep. 2017;7:44373.
[55] Hayes JD, Dinkova-Kostova AT, Tew KD. Oxidative stress in cancer. Cancer Cell. 2020;38:167–197.
[56] Li Y, Xue Y, Xu X, et al. A mitochondrial FUNDC1/HSC70 interaction organizes the proteostatic stress response at the risk of cell morbidity. Embo J. 2019;38:e98786.
[57] Brenner S. The genetics of *Caenorhabditis elegans*. Genetics. 1974;77:71–94.
[58] Kamath RS, Martinez-Campos M, Zipperlen P, et al. Effectiveness of specific RNA-mediated interference through ingested double-stranded RNA in *Caenorhabditis elegans*. Genome Biol. 2000;2(1);1–10.
[59] Bratic I, Hench J, Trifunovic A. *Caenorhabditis elegans* as a model system for mtDNA replication defects. Methods. 2010;51:437–443.
[60] Wojtovich AP, Burwell LS, Sherman TA, et al. The *C. elegans* mitochondrial K+ATP channel: A potential target for preconditioning. Biochem Biophys Res Commun. 2008;376:625–628.
[61] Dean CB, Nielsen JD. Generalized linear mixed models: a review and some extensions. Lifetime Data Analysis. 2007;13(4):497–512.
[62] Love MI, Huber W, Anders S. Moderated estimation of fold change and dispersion for RNA-seq data with DESeq2. Genome Biol. 2014;15:550.
[63] Zhang J, Wang YT, Miller JH, et al. Accumulation of succinate in cardiac ischemia primarily occurs via canonical krebs cycle activity. Cell Rep. 2018;23:2617–2628.
[64] Xia J, Wishart DS. Web-based inference of biological patterns, functions and pathways from metabolomic data using MetaboAnalyst. Nat Protoc. 2011;6:743–760.